IEEE Access
Multidisciplinary | Rapid Review | Open Access Journal

Received January 9, 2018, accepted February 2, 2018, date of publication February 27, 2018, date of current version April 4, 2018.

Digital Object Identifier 10.1109/ACCESS.2018.2808298

Numerical Analysis of the Water Film Characteristics in the Eccentric State of a Radial Piston Pump

JIANG QUAN[1,2,3], YANG HONGBO[1,3], YU YONG[3], AND CAI LIMING[3], AND CHENG XIANKAI[3]

[1]Changchun Institute of Optics, Fine Mechanics and Physics, Chinese Academy of Sciences, Changchun, 130033, China
[2]University of Chinese Academy of Sciences, Beijing 100039, China
[3]Suzhou Institute of Biomedical Engineering and Technology, Chinese Academy of Sciences, Suzhou, 215163, China

Corresponding author: Jiang Quan (jiangqrh@163.com)

This work was supported in part by the major special projects of the army during 12th Five-year Plan, one-stop continuous blood purification device and multi-functional in vitro life support system research under Grant AWS11J03 and in part by the Suzhou medical equipment special projects.

ABSTRACT This paper investigates the working efficiency and reliability of a piston pair of radial piston pumps by accurately calculating the shape and pressure distribution of the piston pair. First, a leakage model of the piston pair is established based on the equivalent liquid resistance and adaptive eccentricity. This model considers the piston micro-motion in the cylinder and the force balance. Then, the piston clearance shape and pressure distribution are numerically simulated using a genetic algorithm and the finite-volume method, and the clearance leakage flow is discussed. The example analysis demonstrates the accuracy of the model; the iterative algorithm has good numerical stability at the given precision and can rapidly converge to the global optimal solution of the model to obtain the real-time piston eccentricity state and pressure distribution with high accuracy. The results demonstrate that the model has high accuracy. Finally, the effects of various parameters such as the piston diameter, initial clearance of the piston pairs, and piston speed on the leakage rate are discussed. The conclusions of this paper provide guidance for the design of water piston pumps.

INDEX TERMS Equivalent liquid resistance, leakage, piston pump, pressure distribution, self-adaptive eccentricity.

I. INTRODUCTION

The piston pump is a mechanical device that is used to convert mechanical energy into fluid pressure. As an important member of the pump family, the radial piston pump [1]–[4] has high efficiency, high working pressure, high reliability and a long lifespan [5]–[7]. The life and efficiency of the pump are affected by the pressure distribution and leakage flow of the piston pair, which consists of the piston and cylinder. The pressure distribution and leakage flow are closely related to the piston clearance shape, which is influenced by the piston eccentricity. The piston eccentricity is formed by the incline and the offset relative to the axis of the cylinder during the reciprocating motion of the piston.

Kumar and Bergada [8] analyzed the relationship between the piston clearance, leakage flow and torque of the piston. Bergada textitet al. [9] used a pressure equalizer groove to study the pressure of the piston oil film. Pelosi and Ivantysynova [10] and [11] analyzed the kinematics of the piston and friction of the oil film and improved the oil film lubrication characteristics of the piston by changing the surface shape of the piston. Garrett [12] studied the effect of the piston material on the thermal deformation of the piston and found that the oil film shape determined the working state of the pump. Using simulations, Wieczorek and Ivantysynova [13] found that the piston eccentricity could influence the pressure on the piston oil film. Sadashivappa *et al.* [14] investigated the performance of the oil film of the elliptical piston and provided a new idea for the design of the piston pump and motor. Fang and Shirakashi [15] examined the characteristics of the oil film lubrication of the piston and found that the thickness of the oil film decreased as the pump speed increased. Deeken [16] constructed virtual prototypes to study the microscopic characteristics of the oil film. Ma *et al.* [17] analyzed wear behavior of swash plate/slipper pair of axis piston hydraulic pump based on EHL model. Xu *et al.* [18] studied the micro-motion of the piston in the

cylinder and found that the piston eccentricity caused by the micro-motion of the piston affected the oil film characteristics.

Qian and Liao [19] considered a nonisothermal fluid-solid coupling model of the piston leakage flow. Mihailidis *et al.* [20] present a new line contacts model, which considers the thermal effects and the non-Newtonian lubricant behavior, to investigate the influence of the lubricant on the pressure distribution and film shape. Zhou *et al.* [21] proposed a point contact lubrication model which considers the non-Newtonian thermal elastohydrodynamic lubrication (EHL) theory for a crowned herringbone gear drive, and investigated the effects of the major geometry and working parameters on the lubrication performance. Yang *et al.* [22] proposed a Reynolds equation for a general lubrication problem for the non-Newtonian fluid through regarding the lubricant flow as a superposition of Poiseuille flow and Couette flow. Lin *et al.* [23] investigated the power-law film slider bearings with the Rabinowitsch fluid model by deriving a two-dimensional non-Newtonian Reynolds equation.

Yang *et al.* [24]–[29] proposed a new integral transform method to find the solution for the differential equation, and the method can be applied to solve some partial differential equations. Qian and Liao [30] analyzed the piston force by numerically solving the pressure balance equation of the piston and studied the valve eccentric oil film characteristics. However, it is difficult to establish the relationship between the leakage of the piston pair and the adaptive eccentricity of the piston.

Therefore, this paper aims to simulate the piston micro-motion, pressure distribution of the piston pair, and leakage flow at different angular positions of the eccentric wheel. We develop a fully coupled fluid-structure mathematical model that considers the adaptive eccentricity that is caused by piston micro-movement and equivalent hydrodynamic resistance of the water film thickness. This model is solved using a numerical method that can simultaneously obtain the pressure distribution and leakage rate.

II. MATHEMATICAL MODEL AND SOLUTION TECHNIQUE

A. HYDRODYNAMIC EQUATION

A general lubrication system in the Cartesian coordinate system is studied. For a common non-Newtonian fluid, the viscosity decreases as the shear stress increases over a certain range of shear stress. A variety of mathematical models can be used to describe this behavior. Among them, the power law model has been widely used because of its simplicity in the limited range of shear rate. The relationship between the shear stress and shear rate is nonlinear for non-Newtonian fluids, and the general form can be written as:

$$\tau = \phi\gamma^n \tag{1}$$

where γ is shear rate and τ is shear stress. Φ is a dimensional constant, whose dimension depends on the power law index n.

The non-Newtonian behavior and contact friction effect are included. The pressure distribution in the contact domain is governed by the modified Reynolds equation, which can be written as:

$$\frac{\partial}{\partial x}(\rho h^2(\frac{h}{\phi}\frac{\partial p}{\partial x})^{\frac{1}{n}}) + \frac{\partial}{\partial y}(\rho h^2(\frac{h}{\phi}\frac{\partial p}{\partial y})^{\frac{1}{n}}) = \frac{2^{1+\frac{1}{n}}(2n+1)}{n}\cdot(\frac{\partial}{\partial x}\frac{V_{S\theta}\rho h}{2} + \frac{\partial}{\partial y}\frac{V_{SL}\rho h}{2} + \frac{\partial(\rho h)}{\partial t}) \tag{2}$$

In Eq.(2), ρ is the lubricant density; p is the oil film pressure; Φ is the dynamic viscosity; $V_{S\theta}$ and V_{SL} are the film axis velocities on the piston and cylinder surfaces, respectively; h is film thickness; and t is time.

The parameter n is an index that measures the non-Newtonian behavior of a fluid. Normally, n is less than 1 or n is greater than 1. When $n = 1$, the model degenerates into a Newtonian fluid lubrication model. The theoretical values of the non-Newtonian parameter has been selected by the method in the available literature and obtained through experiment.

B. FORCE ANALYSIS OF THE PISTON

The piston causes eccentricity in the cylinder because of the uneven force that is generated when the piston moves. The force condition of the piston is shown in Figure 1.

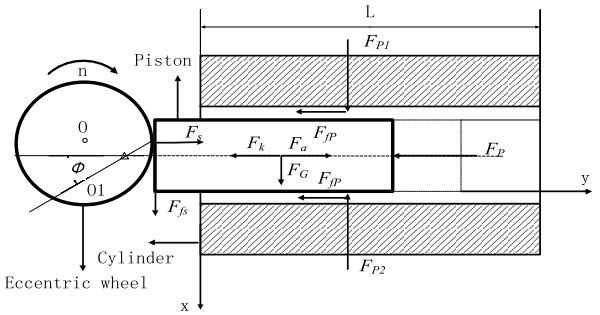

FIGURE 1. Stress analysis of the piston.

In the plane of rotation of the eccentric wheel, the X and Y axes are defined as the axial direction of the piston and the direction perpendicular to the piston, respectively. Then, the force balance equation and moment balance equations of the piston in the X and Y directions are:

$$F_s - F_{fP} + F_a - F_{PP} - F_k = 0 \tag{3}$$

$$f_2 F_s + F_G + F_{px} = 0 \tag{4}$$

$$M_{F_S} + M_{F_G} + M_{F_P} = 0 \tag{5}$$

where F_s is the supporting force of the eccentric wheel to the piston; F_{fs} is the friction force of the eccentric wheel to the piston; F_a is the inertial force of the piston; F_k is the elastic force of the return spring to the piston; F_{PP} is the piston drainage chamber pressure; F_{fP} is the friction of the water film to the piston; F_G is the gravity of the piston; F_{Py} is the dynamic support force of the submerged piston membrane, which acts at the location where the cylinder comes into

contact with the surface of the piston and acts along the piston surface to the column plug axis; Φ is the rotation angle of the eccentric wheel; and M_{FS}, M_{FG}, and M_P are the torques of the external force.

At any point in the piston movement, the external forces F_s, F_a, F_k, F_{PP}, and F_G of the piston can be calculated using the above parameters. The dynamic bearing force F_P of the submerged piston film is affected by the shape of the submerged water film. At different positions of the piston, the piston pair produces different water film shapes, which correspond to different dynamic pressure support forces to satisfy the balance force of the piston pair. Figure 1 shows the piston sub-clearance diagram, the piston eccentric state, and the piston axis tilt. The relative movement of the piston and cylinder are equivalent to the relative movement of two non-parallel planes before and after the pressure difference. The clearance between the water film will produce a dynamic pressure.

F_{Py} can be obtained by a radial positive pressure integral that acts on the surface of the piston:

$$F_{px} = \iint p(x, y)\cos(\alpha)dxdy \tag{6}$$

where

$$p(x, y) = p_h(x, y) + p_c(x, y) \tag{7}$$

where P_h is the fluid support hydraulic pressure of the piston and Pc is the solid contact pressure. In the mixed friction region, the pressure distribution consists of the fluid pressure P_h and the solid contact pressure Pc. The fluid pressure P_h at any point on the piston surface that is caused by the dynamic pressure bearing is expressed as:

$$p_k = \frac{\frac{6\mu VL}{h_2^2(h_2-h_1)}}{h_1+(h_2-h_1)\frac{x}{L}} - \frac{\frac{6\mu VLh_1h_2}{(h_2+h_1)} + \frac{h_1^2h_2^2(p_s-p_o)}{(h_2+h_1)}}{(h_2-h_1)\left[h_1+(h_2-h_1)\frac{x}{L}\right]^2} + \frac{p_s(h_2^2-h_1^2)+h_1^2(p_s-p_o)-6\mu UL}{(h_2-h_1)(h_2+h_1)} \tag{8}$$

where p_k is the dynamic pressure caused by the dynamic pressure support, μ is the viscosity of the liquid, V is the velocity of the piston, L is the remaining length of the piston in the cylinder, i.e., the seal length of the piston, and x is the point coordinate. Figure 2 shows that h_1 and h_2 are the water film thicknesses at the two ends of the piston, and p_1 and p_2 are the pressures at the two ends.

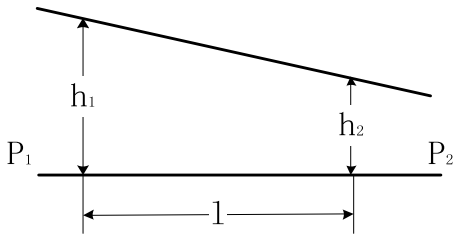

FIGURE 2. Equivalent model of clearance.

The solid contact pressure P_c is expressed as:

$$\bar{p}_c(x, y) = \frac{1}{\Omega}\int_{(\Omega)} p_c(x, y)d\Omega \tag{9}$$

where $p_c(\theta, L)$ is the contact pressure at any point on the piston surface.

$$p_c(x, y) = f[w_{el}(x, y) + w_{pl}(x, y)] \tag{10}$$

where w_{el} is elastic deformation and w_{pl} is plastic deformation.

$$w_{el}(x, y) = \frac{1}{\pi E_{com}}\iint \frac{p_c(x', y')dx'dy'}{\sqrt{(x-x')^2+(y-y')^2}} \tag{11}$$

where E_{com} is the comprehensive Young's modulus of the piston and the cylinder.

C. ANALYSIS OF THE PISTON CLEARANCE

The contact of the piston and cylinder occurs mainly in the points of contact at both ends. As such, the clearance of the piston and cylinder, which is considered the point contact model, can be expressed as:

$$h(x, y) = h_h(x, y) + h_c(x, y) \tag{12}$$

h_h(x,y) is the clearance considering the deformation of the piston and the cylinder with non contact.

$$h_h(x, y) = h_e(x, y) + \Delta h_1(x, y) + \Delta h_2(x, y) \tag{13}$$

where Δh_1 and Δh_2 are the radial swell of the cylinder bore and the radial decrease of the piston outer surface caused by the fluid pressure, respectively. According to Lame's formula for a thick-walled cylinder, the deformations are given as:

$$\Delta h_1 = p\frac{d}{2E}\left(\frac{d_0^2+d^2}{d_0^2-d^2}+\upsilon\right) \tag{14}$$

$$\Delta h_2 = p\frac{d}{2E} - p_L\frac{d}{2E}\upsilon \tag{15}$$

where d_0 is the outer diameter of the cylinder. The second term that includes P_L in Eq. (12) is the piston radial Poisson deformation, neglecting the inertia force acting on the piston.

$h_e(x,y)$ is the initial clearance considering the real-time eccentricity and offset of the piston. As shown in Figure 3, considering the possible inclination and eccentricity of the piston in the cylinder, the piston clearance is:

$$h_e(x, y) = h_0 - e(\theta, e, y)\cdot\cos(\alpha) \tag{16}$$

where h_0 is the initial clearance when the piston is concentric to the cylinder, e is the eccentricity and θ is the offset of the piston, and α is the coordinate in the circumferential direction.

The inclination and eccentricity of the piston in the cylinder are denoted by θ and e, respectively. The piston eccentricity at different positions on the piston circumference is expressed as

$$e(\theta, e, y) = (0.5L - y)\cdot\tan(\theta) + e \tag{17}$$

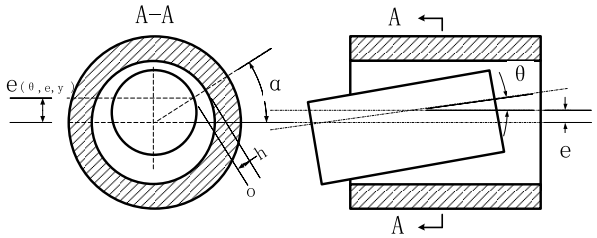

FIGURE 3. Piston position in the cylinder.

where L is the piston seal length, which changes cycle because of the sine reciprocating motion of the piston.

$h_c(x,y)$ indicates the effect of contact deformation on the piston clearance.

$$h_c(x,y) = \frac{x^2}{2R_x} + \frac{y^2}{2R_y} + w_{el}(x,y) \tag{18}$$

where w_{el}(x,y) is elastic deformation of contact point, R_x, R_y, are the reduced radius of curvature of an equivalent cylindrical.

D. NUMERICAL SOLUTION

For Eq. (2), $V_{S\theta} = 0$, because there is no rotational motion of the piston in the cylinder. Without considering the squeezing effect of the liquid, the right side of the equation is reduced to only the axial velocity V_{SL}:

$$\frac{\partial}{\partial x}(\rho h^2(\frac{h}{\phi}\frac{\partial p}{\partial x})^{\frac{1}{n}}) + \frac{\partial}{\partial y}(\rho h^2(\frac{h}{\phi}\frac{\partial p}{\partial y})^{\frac{1}{n}}) = \frac{2^{1+\frac{1}{n}}(2n+1)V_{SL}}{2n} \cdot (\frac{\partial \rho h}{\partial y}) \tag{19}$$

In order to facilitate an iterative solution, the non-dimensional Rayleigh equation is:

$$\frac{\partial}{\partial X}(\varepsilon_X \frac{\partial P}{\partial X})dXdY + \frac{\partial}{\partial Y}(\varepsilon_Y \frac{\partial P}{\partial Y})dXdY = \frac{\partial(\rho^* H)}{\partial Y} \tag{20}$$

where

$$\varepsilon_X = k\rho H^2(\frac{H}{\phi})^{\frac{1}{n}}(\frac{\partial P}{\partial X})^{\frac{1}{n}-1}, \quad \varepsilon_Y = k\rho H^2(\frac{H}{\phi})^{\frac{1}{n}}(\frac{\partial P}{\partial Y})^{\frac{1}{n}-1},$$
$$k = \frac{2n}{2^{1+\frac{1}{n}}(2n+1)V_{SL}}$$

The pressure boundary conditions are:

$$P(Y=0) = P_0; \quad P(Y=L) = P_L;$$

In this paper, the finite-volume method is used to calculate the pressure distribution of the secondary water film. The speed of the integral operation has been improved greatly though using a method provided in the literature [24].

The lubrication area of the piston seal band is meshed in the circumferential and radial directions, and the half-grid range region around the grid node is defined as the limited control volume, as shown in Figure 4.

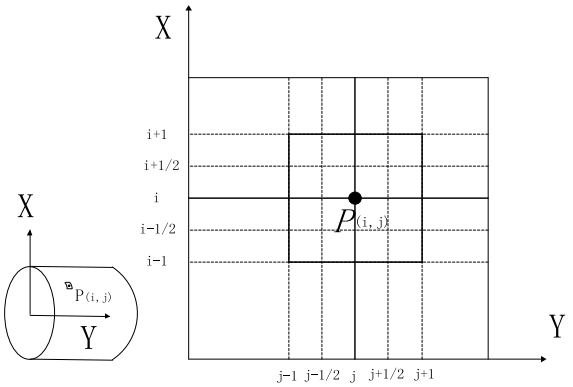

FIGURE 4. Schematic of the staggered mesh discretization.

Both sides of the equation along the axial and radial discretization and the second integral can be obtained:

$$\begin{aligned}&\varepsilon_{i-1/2,j}P_{i-1,j} + \varepsilon_{i+1/2,j}P_{i+1,j} + \varepsilon_{i,j-1/2}P_{i,j-1} \\ &\quad + \varepsilon_{i,j+1/2}P_{i,j+1} - \varepsilon_0 P_{i,j} \\ &\quad = 2\pi R(\rho^*_{ij}H_{ij} - \rho^*_{i-1,j}H_{i-1j})\end{aligned} \tag{21}$$

where

$$\varepsilon_{i\pm1/2,j} = \frac{1}{2}[(\varepsilon_X)_{i,j} + (\varepsilon_X)_{i\pm1,j}],$$
$$\varepsilon_{i,j\pm1/2} = \frac{1}{2}[(\varepsilon_Y)_{i,j} + (\varepsilon_Y)_{i\pm1,j}]$$
$$\varepsilon_0 = \varepsilon_{i+1/2,j} + \varepsilon_{i-1/2,j} + \varepsilon_{i,j+1/2} + \varepsilon_{i,j-1/2}$$

The discretized film thickness H is:

$$H_{i,j} = H_h(X_i, Y_j) + \frac{X_i^2 + Y_j^2}{2} + \frac{2}{\pi E_{com}}\sum_{s=1}^{n}\sum_{t=1}^{n} p_{st}K_{ij}^{kl} \tag{22}$$

where. H_{ij} and P_i are the film thickness and pressure of the P(i,j), respectively, and K_{ij}^{kl} is the stiffness coefficient of elastic deformation.

The iterative computation contains two coupling layers because the piston offset and tilt couple with the force balance equation of the piston, and the piston clearance couples with the pressure distribution of the piston pair. The outer iteration layer adjusts the force balance in Eq. (4) to attain the accuracy of the iterative error by changing the piston offset and tilt angle. When the inner iteration is used to calculate the position of the piston, the pressure distribution of the piston pair is two times less than the specified value. In this paper, the genetic algorithm is used to solve the force balance equation, and the finite-difference method is used to solve the pressure distribution of the piston pair. The solving process is shown in Figure 5.

E. SOLVING PROCESS OF THE GENETIC ALGORITHM

The genetic algorithm (GA) is a random search algorithm that draws on the natural selection and natural genetic mechanism of biology, which is highly suitable for solving complex and nonlinear problems [19]–[21]. The main concept of the GA

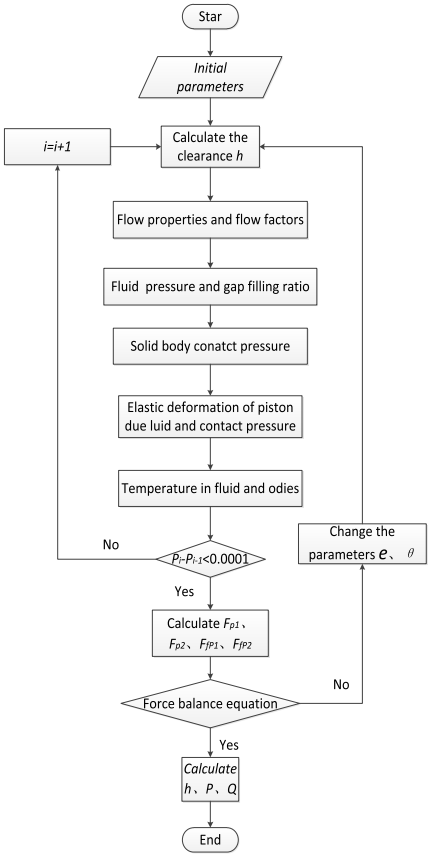

FIGURE 5. Solution trend.

is to code the solved problem and then generate a certain-sized population with a reasonable fitness function to assess gene performance; on this basis, the population can be copied, crossed and mutated.

The objective function is g, and the decision variables are e and θ. Because the piston offset and tilt angle are typically small, the constraints are $0 \leq e \leq 1$ μm and $0 \leq \theta \leq 0.0001$ rad. The initial population was generated using a random distribution. The iteration ends when the objective function value of the optimal individual in the population is less than 0.001.

III. MODEL VALIDATION AND DISCUSSION

Numerical calculations were performed for the radial piston pump. The structural parameters, material properties of the piston pair and operating conditions of the pump are listed in Table 1.

TABLE 1. Input parameters of the model.

Parameters	Value
D/mm	6
h0/um	3
L/mm	10
E/mm	5.3
PL/MPa	5

Figure 6 plots the velocity and inclination of the piston versus the eccentric wheel angle for a rotational speed of 1,000 rpm.

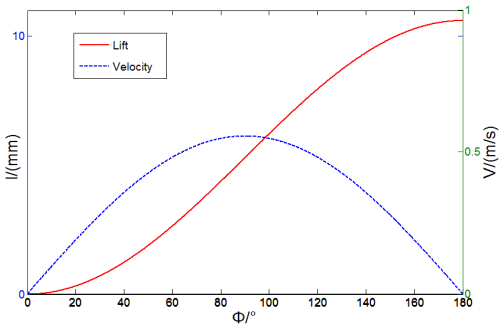

FIGURE 6. Piston lift and velocity versus eccentric wheel angle.

Figure 7 shows the trend and average of the objective function value of the optimal solution in the iteration process of the GA for an eccentric wheel angle of Φ=*0*°. The optimal solution, which was obtained after 51 iterations of the GA, is *e0=0.928* μm and θ *=0.000299*.

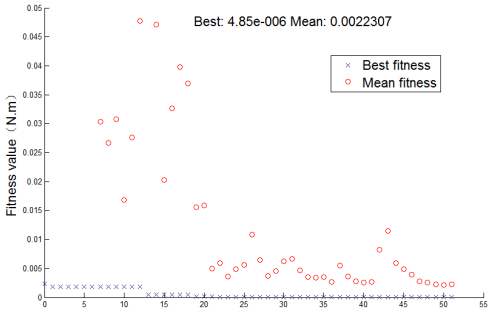

FIGURE 7. Solution trend.

Figure 8 shows that the offset of the piston significantly affects the leakage. For example, the leakage rate of the piston at an offset of 5 μm is approximately 3 times that of an offset of 2 μm. In contrast, the incline of the piston does not considerably affect the leakage. A possible reason for this is the very small allowable incline angle due to the extremely small ratio of the radial clearance to the axial sealing length.

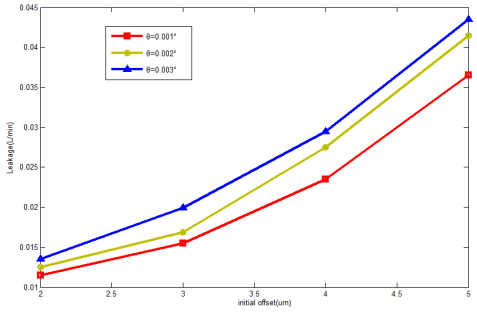

FIGURE 8. Adaptive eccentric state analysis of the piston.

Figure 9 shows the change in the piston self-adaptive eccentric state when the speed is 1,000 rpm. In Figure 9, the dot is the piston offset (unit: *um*), and the point is the piston inclination (unit: rad).

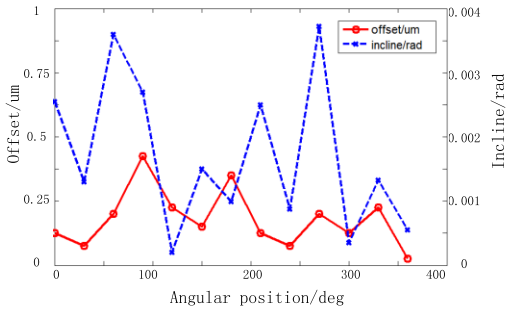

FIGURE 9. Analysis of the adaptive eccentric state of the piston.

In this study, two numerical models are considered: the self-adaptive eccentric (SAE) model and the complete eccentric (CE) model. The SAE varies with the position of the piston and satisfies the constraints of the force balance condition. The adaptive eccentricity of the piston, which is consistent with the instantaneous micro-motion of the piston in the cylinder, can be obtained using the GA and finite-volume technique and is close to the actual situation. The CE model also uses the finite-volume method but assumes that the central clearance is h_0, the minimum clearance of the edge is 0.1 μm, and the piston is in a fully eccentric state. The minimum clearance of the CE model is always 0.1 μm, whereas the minimum clearance of the SAE model may vary between 0.1 μm and h_0 μm. The CE model assumes that there is only incline, and no offset. As shown in Figure 10, the leakage flow is affected more by the offset than by the incline; thus, the leakage of the CE model is relatively small.

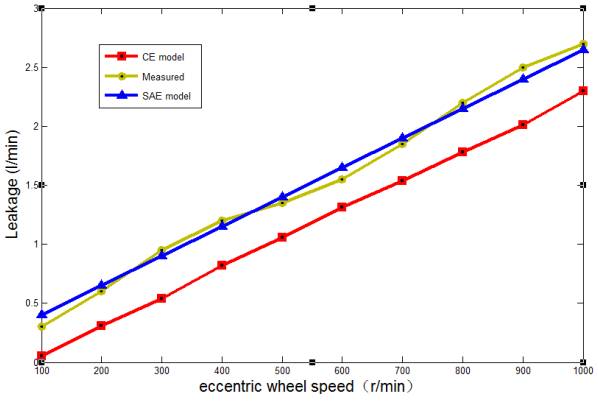

FIGURE 10. Leakage rate versus eccentric wheel speed.

We compared the numerical analysis results and measurements to validate the model. Figure 10 shows the measured and calculated leakage rates versus the eccentric wheel speed. The SAE model established in this study accurately describes the physical phenomena that occur in the piston pair and can predict the leakage rate with good accuracy. The simulation results are consistent with the experimental data, demonstrating the reliability of the model.

The leakage rates calculated using the SAE model are considerably higher than those calculated using the CE model. The effects of the structure and operating parameters of the pump on the leakage rate will be discussed next.

Figure 11 shows the pressure distribution of two different models and three different non-Newtonian parameters (n =0.7, 0.8, and 0.9), for a piston angular position of 90°, an initial clearance of 3 μm, an outlet pressure of 7 MPa and a rotational speed of 1,000 rpm. The fluid pressure calculated using the SAE model decreases slowly from the top edge to the end edge of the seal, which is notably different from the results obtained using the CE model. The smaller n is, the more obvious the shear thinning of the fluid and the lower the viscosity of the lubricant. For the same calculation conditions, the smaller n is, the smaller the load capacity of the lubricating film under the condition of the same film thickness distribution; that is, the corresponding pressure distribution will also be smaller.

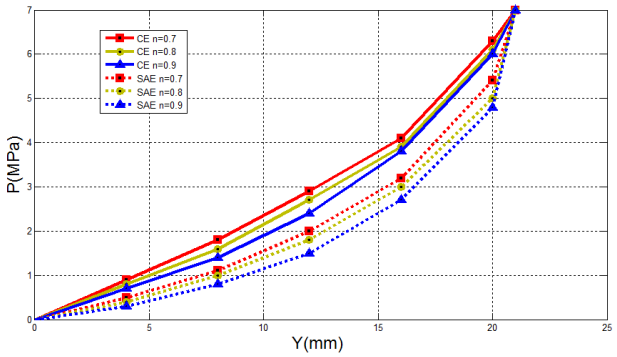

FIGURE 11. Pressure distributions in the axial direction (L=20.6 mm).

The following discussion mainly focuses on the change in the overall piston leakage and pressure distribution of the piston pair with variations in the outlet pressure, speed and initial seal clearance. The overall leakage is obtained by integrating the temporal leakage in Figure 11 as a function of the angular position. Figures 12-15 show the changes in the leakage flow for different piston parameters.

Figure 12(a) shows the leakage rate in the piston pair assembly versus the eccentric wheel angular position for an initial clearance of 3 μm and a turning speed of 1,000 rpm. Three different piston diameters of 4, 6 and 8 mm were considered. Figure 12(a) shows that larger piston diameters correspond to more leakage.

Figure 12(b) shows the effect of the piston diameter on the total leakage flow. The leakage rate increases rapidly with changes in the piston diameter. The ratio of the leakage rates of the SAE and CE models slowly decreases from 2.3 to 1.2 when the piston diameter increases from 3 mm to 8 mm. With the increase in diameter, the SAE model has a slower

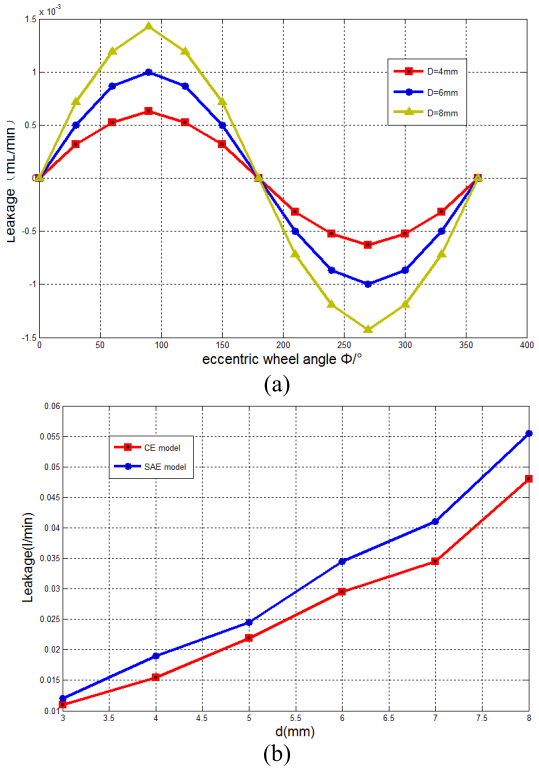

FIGURE 12. Leakage rate versus piston diameter. (a) Instantaneous leakage rate. (b) Total leakage rate.

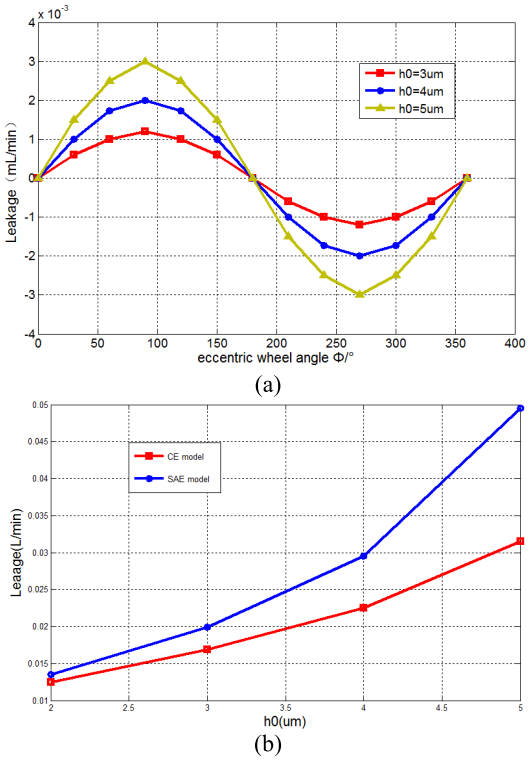

FIGURE 13. Leakage rate versus initial clearance. (a) Instantaneous leakage rate. (b) Total leakage rate.

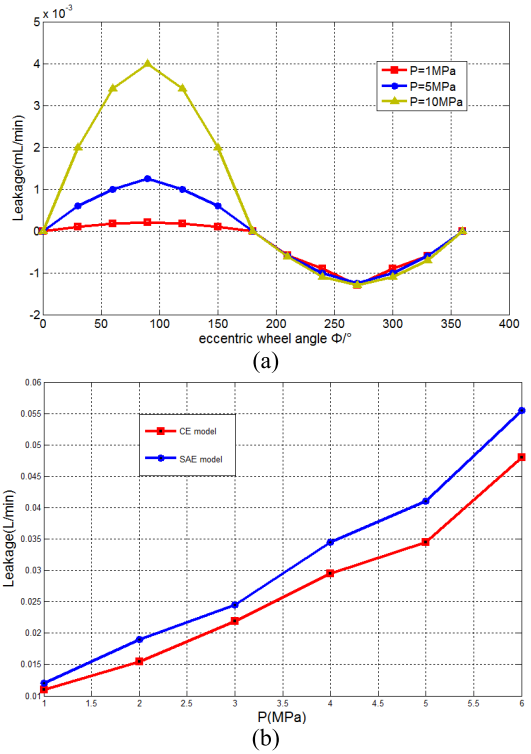

FIGURE 14. Leakage rate flow of the piston at different speeds. (a) Instantaneous leakage rate. (b) Total leakage rate.

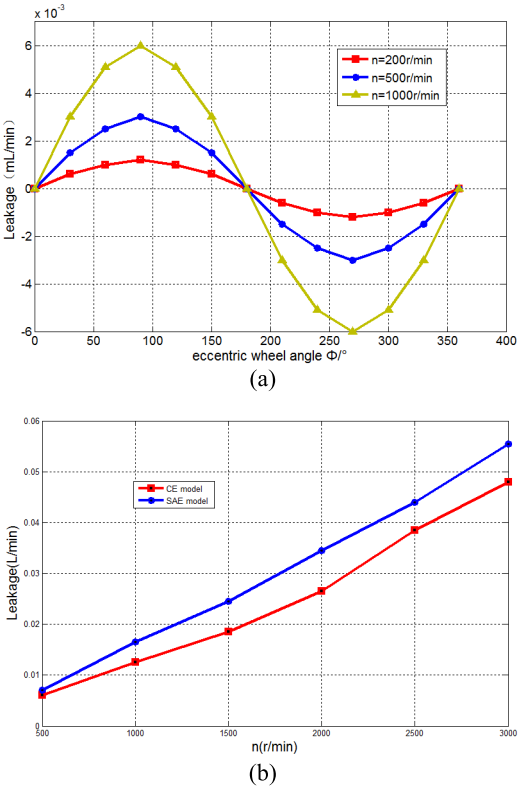

FIGURE 15. Leakage rate versus piston cylinder pressure. (a) Instantaneous leakage rate. (b) Total leakage rate.

leakage rate than the CE model, which indicates that the diameter of the piston has a greater effect because the CE model assumes that the clearance of the secondary edge of the piston is minimal. When the piston diameter increases, the incline of the piston is aggravated, and the leakage of the piston increases.

Figure 13(a) shows the leakage rate in the piston pair assembly versus the eccentric wheel angular position for an initial clearance of 3 μm and a cylinder pressure of 2 MPa. Three different initial clearances were considered: 3, 4 and 5 μm. As shown in Figure 13(a), a larger initial piston clearance corresponds to a larger leakage flow because the initial clearance of the piston determines the average piston clearance, and larger pistons have greater leakage.

Figure 13(b) shows that the total leakage rate calculated using the SAE model doubles when the piston clearance increases from 2 μm to 5 μm. The difference between the SAE model and CE model increases as the initial clearance of the piston increases. The leakage flow of the SAE model is approximately 1.1 and 1.9 times that of the CE model when the clearance is $h_0 = 2$ and $h_0 = 5$, respectively. Therefore, the SAE model is more accurate when the initial clearance of the piston is large.

Figure 14(a) shows the leakage rate in the piston pair assembly versus the eccentric wheel angular position for an initial clearance of 3 μm and a turning speed of 1,000 rpm. Three different cylinder pressures were considered: 2, 5 and 10 MPa.

The piston leakage varies under different export pressure conditions. The piston clearance is related to the positive pressure of the piston, and the forward pressure increases with the outlet pressure of the piston chamber. Therefore, the piston leakage rate increases as the outlet pressure increases.

Figure 14(b) shows the effect of the piston outlet pressure on the total leakage rate flow. As shown in the figure, the piston total leakage flow increases as the outlet pressure increases. In addition, the difference between the CE and SAE models increases as the export pressure increases.

Figure 15(a) shows the leakage rate in the piston-pair assembly versus the eccentric wheel angular position for an initial clearance of 3 μm and a cylinder pressure of 2 MPa. Three pump turning speeds were considered: 200, 500 and 1,000 rpm. When the piston is connected to the higher-pressure side, the leakage is affected by the turning speed because the Couette flow, which is related to the piston velocity, is higher than the Poiseuille flow.

Figure 15(b) shows the effects of different outlet pressures and motor speeds on piston leakage. The piston leakage flow increases with increasing motor speed. The pressure difference causes Poiseuille flow, which causes Couette flow. The piston velocity does not considerably affect the leakage flow when the pressure difference is large. However, the maximum pressure of the piston chamber is 10 MPa, and thus, the piston leakage flow increases as the motor speed increases. The leakage increases more rapidly at lower piston chamber pressures.

IV. CONCLUSIONS

In this paper, we conducted a simulation to observe the influence of structural and operating parameters on pressure distribution and leakage. The piston diameter D, speed n, pressure P and initial clearance h_0 were varied in the simulation.

The following conclusions are drawn from the results of this study:

1) The piston in the cylinder has a certain micro-movement, which causes eccentricity of the piston and cylinder. This eccentricity in turn causes the piston clearance to vary continuously. As a result, the pressure distribution of the piston is uneven.
2) The piston clearance and motor speed significantly affect the performance of the piston pump, whereas the initial sealing length, piston diameter and piston eccentricity do not considerably affect the leakage of the piston.
3) The calculation example demonstrates that the outlet pressure, motor speed and initial sealing clearance are closely related to the pressure distribution, dynamic pressure effect and clearance change during piston movement. These parameters considerably affect the leakage flow of the piston.
4) The hydrodynamic characteristics of the water film are highly sensitive to the overall offset and incline of the piston. The hydrodynamic characteristics of the water film are more sensitive to the piston incline than the offset. The overall offset of the piston greatly affects leakage, whereas the incline does not considerably affect leakage flow.
5) The numerical simulation results that are based on the Reynolds equation and force balance equation are consistent with the experimental results, to a certain extent. However, there are some errors. The error of the theoretical numerical solution mainly originates from the simplification of the calculation model and the precision control of the iterative operation.
6) Future studies will focus on the grooves on the piston face and their effects on fluid characteristics.

REFERENCES

[1] E. Chappel, S. Mefti, G.-L. Lettieri, S. Proennecke, and C. Conan, "High precision innovative micropump for artificial pancreas," *Proc. SPIE*, vol. 8976, no. 2, pp. 89761C-1–89761C-12, Mar. 2014.
[2] M. S. B. Ibrahim and M. M. B. Mahat, "CFD analysis of electromagnetic based valveless pump," *Procedia Eng.*, vol. 41, pp. 1524–1532, Jul. 2012.
[3] C. von Kuensberg Sarre, S.-C. Kong, and R. D. Reitz, "Modeling the effects of injector nozzle geometry on diesel sprays," SAE Tech. Paper 1999-01-0912, 1999.
[4] J. Yang, "Fluid dynamics of axial piston seal," *Ind. Lubrication Tribol.*, vol. 62, no. 1, pp. 12–15, Feb. 2010.
[5] A. E. Catania and A. Ferrari, "Experimental analysis, modeling, and control of volumetric radial-piston pumps," *J. Fluids Eng.*, vol. 133, no. 8, pp. 081103-1–081103-12, Aug. 2011.
[6] A. T. Al-Halhouli, M. I. Kilani, and S. Büttgenbach, "Development of a novel electromagnetic pump for biomedical applications," *Sens. Actuators A, Phys.*, vol. 162, no. 2, pp. 172–176, Aug. 2010.
[7] W. Jiang, Z. Zheng, Y. Zhu, and Y. Li, "Demodulation for hydraulic pump fault signals based on local mean decomposition and improved adaptive multiscale morphology analysis," *Mech. Syst. Signal Process.*, vols. 58–59, pp. 179–205, Jun. 2015.
[8] S. Kumar and J. M. Bergada, "The effect of piston grooves performance in an axial piston pumps via CFD analysis," *Int. J. Mech. Sci.*, vol. 66, pp. 168–179, Jan. 2013.
[9] J. M. Bergada, S. Kumar, D. L. Davies, and J. Watton, "A complete analysis of axial piston pump leakage and output flow ripples," *Appl. Math. Model.*, vol. 36, no. 4, pp. 1731–1751, Apr. 2012.

[10] M. Pelosi and M. Ivantysynova, "Heat transfer and thermal elastic deformation analysis on the piston/cylinder interface of axial piston machines," *J. Tribol.*, vol. 134, no. 4, pp. 041101-1–041101-15, Aug. 2012.
[11] M. Pelosi and M. Ivantysynova, "A geometric multigrid solver for the piston–cylinder interface of axial piston machines," *Tribol. Trans.*, vol. 55, no. 2, pp. 163–174, 2012.
[12] R. A. Garrett, "Investigation of reducing energy dissipation in axial piston machines of swashplate type using axially waved pistons," Ph.D. dissertation, School Mech. Eng., Purdue Univ., West Lafayette, IN, USA, 2009.
[13] U. Wieczorek and M. Ivantysynova, "Computer aided optimization of bearing and sealing gaps in hydrostatic machines—The simulation tool caspar," *Int. J. Fluid Power*, vol. 3, no. 1, pp. 7–20, Jan. 2002.
[14] K. Sadashivappa, M. Singaperumal, and K. Narayanasamy, "On the efficiency of the axial piston motor considering piston form deviations," *Mechatronics*, vol. 6, no. 3, pp. 283–301, Apr. 1996.
[15] Y. Fang and M. Shirakashi, "Mixed lubrication characteristics between the piston and cylinder in hydraulic piston pump-motor," *J. Tribol.*, vol. 117, no. 1, pp. 80–85, Jan. 1995.
[16] M. Deeken, "Simulation of the reversing effects of axial piston pumps using conventional CAE tools," *Ölhydraulik und Pneumatik (O+P)*, vol. 6, pp. 6–12, 2002.
[17] J. Ma, J. Chen, J. Li, Q. Li, and C. Ren, "Wear analysis of swash plate/slipper pair of axis piston hydraulic pump," *Tribol. Int.*, vol. 90, pp. 467–472, Oct. 2015.
[18] B. Xu, J. Zhang, H. Yang, and B. Zhang, "Investigation on the radial micromotion about piston of axial piston pump," *Chin. J. Mech. Eng.*, vol. 26, no. 2, pp. 325–333, Mar. 2013.
[19] D. Qian and R. Liao, "A nonisothermal fluid-structure interaction analysis on the piston/cylinder interface leakage of high-pressure fuel pump," *J. Tribol.*, vol. 136, no. 2, pp. 021704-1–021704-8, Feb. 2014.
[20] A. Mihailidis, K. Agouridas, and K. Panagiotidis, "Non-Newtonian starved thermal-elastohydrodynamic lubrication of finite line contacts," *Tribol. Trans.*, vol. 56, no. 1, pp. 88–100, 2013.
[21] C. Zhou, L. Pan, J. Xu, and X. Han, "Non-Newtonian thermal elastohydrodynamic lubrication in point contact for a crowned herringbone gear drive," *Tribol. Int.*, vol. 116, pp. 470–481, Dec. 2017.
[22] Q. Yang, P. Huang, and Y. Fang, "A novel Reynolds equation of non-Newtonian fluid for lubrication simulation," *Tribol. Int.*, vol. 94, pp. 458–463, Feb. 2016.
[23] J.-R. Lin, L.-M. Chu, T.-C. Hung, and P.-Y. Wang, "Derivation of two-dimensional non-Newtonian Reynolds equation and application to power-law film slider bearings: Rabinowitsch fluid model," *Appl. Math. Model.*, vol. 40, nos. 19–20, pp. 8832–8841, Oct. 2016.
[24] X.-J. Yang, "A new integral transform with an application in heat-transfer problem," *Thermal Sci.*, vol. 20, pp. 677–681, 2016.
[25] X.-J. Yang, "A new integral transform operator for solving the heat-diffusion problem," *Appl. Math. Lett.*, vol. 64, pp. 193–197, Feb. 2017.
[26] X.-J. Yang, J. A. T. Machado, C. Cattani, and F. Gao, "On a fractal LC-electric circuit modeled by local fractional calculus," *Commun. Nonlinear Sci. Numer. Simul.*, vol. 47, pp. 200–206, Jun. 2017.
[27] X. J. Yang and F. Gao, "A new technology for solving diffusion and heat equations," *Thermal Sci.*, vol. 21, no. 1A, pp. 133–140, 2017.
[28] X.-J. Yang, J. A. T. Machado, D. Baleanu, and F. Gao, "A new numerical technique for local fractional diffusion equation in fractal heat transfer," *J. Nonlinear Sci. Appl.*, vol. 9, pp. 5621–5628, 2016.
[29] X. Liang, F. Gao, Y.-N. Gao, and X.-J. Yang, "Applications of a novel integral transform to partial differential equations," *J. Nonlinear Sci. Appl.*, vol. 10, no. 2, pp. 528–534, Feb. 2017.
[30] D. Qian and R. Liao, "Theoretical analysis and mathematical modelling of a high-pressure pump in the common rail injection system for diesel engines," *Proc. Inst. Mech. Eng. A, J. Power Energy*, vol. 229, no. 1, pp. 60–72, Jun. 2014.

JIANG QUAN was born in 1989. He is currently pursuing the Ph.D. degree, mainly engaged in rehabilitation medical equipment research.

YANG HONGBO was born in 1963. He is currently a Researcher and a Ph.D. candidate supervisor, mainly engaged in mechanical and electrical integration, computer simulation design, rehabilitation technology, and other research directions.

YU YONG was born in 1975. He is currently an Associate Researcher and a Supervisor of master's degree students, mainly engaged in mechatronics, image processing, rehabilitation engineering technology, and other research directions.

CAI LIMING was born in 1985. He is currently an Assistant Researcher, mainly engaged in the application of precision machinery, mechanical structure, gas static pressure technology in the field of biomedical engineering.

CHENG XIANKAI was born in 1984. He is currently an Assistant Researcher, mainly engaged in servo control, digital image processing, robot control, and other directions.